Vision Research 114 (2015) 48–55

Contents lists available at ScienceDirect

Vision Research

journal homepage: www.elsevier.com/locate/visres

Altered white matter in early visual pathways of humans with amblyopia

Brian Allen [a], Daniel P. Spiegel [c,d], Benjamin Thompson [c,e], Franco Pestilli [b,1], Bas Rokers [a,*,1]

[a] Department of Psychology, University of Wisconsin-Madison, Madison, WI, United States
[b] Department of Psychological and Brain Sciences, Indiana University, Bloomington, IN, United States
[c] Optometry and Vision Science, University of Auckland, Auckland, New Zealand
[d] McGill Vision Research, Department of Ophthalmology, McGill University, Montreal, Canada
[e] Optometry and Vision Science, University of Waterloo, Canada

ARTICLE INFO

Article history:
Received 8 September 2014
Received in revised form 16 December 2014
Available online 20 January 2015

Keywords:
Amblyopia
White matter
Tractography
Diffusion-MRI

ABSTRACT

Amblyopia is a visual disorder caused by poorly coordinated binocular input during development. Little is known about the impact of amblyopia on the white matter within the visual system. We studied the properties of six major visual white-matter pathways in a group of adults with amblyopia ($n = 10$) and matched controls ($n = 10$) using diffusion weighted imaging (DWI) and fiber tractography. While we did not find significant differences in diffusion properties in cortico-cortical pathways, patients with amblyopia exhibited increased mean diffusivity in thalamo-cortical visual pathways. These findings suggest that amblyopia may systematically alter the white matter properties of early visual pathways.

1. Introduction

Amblyopia is a developmental disorder that occurs when the visual input from the two eyes is poorly correlated during early development. Such poor correlation may be due to a chronically blurred image in one eye (anisometropia), a turned eye (strabismus), or deprivation of one or both eyes. Since visual input is atypical in amblyopia, it is of interest not only as a clinical disorder, but also as a human model of the interplay between sensory input and neural development. Accordingly, amblyopia has been widely studied both neurophysiologically (Hubel & Wiesel, 1970) and psychophysically (Asper, Crewther, & Sheila, 2000).

Amblyopia is associated with impairments in both monocular and binocular vision (McKee, Levi, & Movshon, 2003). Monocular deficits are apparent when patients use only their amblyopic eye, and include impaired spatial acuity (Holmes & Clarke, 2006; Levi & Klein, 1982), reduced contrast sensitivity (Hess & Howell, 1977; Levi & Harwerth, 1978) and impaired performance on tasks requiring the integration of form or motion (for a recent review see Hamm et al., 2014). Binocular visual dysfunction is also common in patients with amblyopia, often resulting in severely degraded or absent sensitivity to binocular disparity (Holmes & Clarke, 2006; Li et al., 2011).

The neuro-anatomical consequences of amblyopia in humans are less established than the functional deficits. There is evidence for reduced grey matter in the lateral geniculate nucleus (LGN) (Barnes et al., 2010; von Noorden, Crawford, & Levacy, 1983), and the primary and extrastriate visual cortex (Chan et al., 2004; Mendola et al., 2005). Whether these structural changes are restricted to grey matter or affect the white matter is an open question, although some evidence for abnormal development of the prechiasmatic pathways (Gümüstas et al., 2013; Pineles & Demer, 2009) and optic radiations has been reported in children with amblyopia (Ming-xia et al., 2007; Song et al., 2010; Xie et al., 2007).

Recent developments in MRI-based diffusion weighted imaging (DWI) and tract-estimating algorithms (called "tractography") provide means to identify the anatomy, location and structural properties of white matter pathways. The ability to identify the general characteristics of these pathways in humans *in vivo* is a crucial step in understanding how visual networks develop. Accordingly, we used a novel DWI protocol that is able to track multiple, potentially intersecting tracts within the visual system, and assessed whether the structural properties of white matter within the visual system differed between controls and participants with amblyopia.

We selected a number of white matter pathways, that connect visual areas known to be affected by amblyopia (LGN, V1 & hMT+). The first pathway of interest was the optic radiation, a

* Corresponding author at: Department of Psychology, University of Wisconsin-Madison, 1202 W Johnson St., Madison, WI 53706, United States. Fax: +1 (608) 262 4029.
E-mail address: rokers@wisc.edu (B. Rokers).
[1] These authors contributed equally to this work and share senior authorship.

http://dx.doi.org/10.1016/j.visres.2014.12.021
0042-6989/

primary thalamo-cortical pathway projecting from the lateral geniculate nucleus to the primary visual cortex. Functional (Hess et al., 2009, 2010; Levi & Harwerth, 1978; Lv et al., 2008; Miki et al., 2003; Mizoguchi et al., 2005) and structural (von Noorden, Crawford, & Levacy, 1983; Movson et al., 1987; Barnes et al., 2010; Chan et al., 2004; Lv et al., 2008; Mendola et al., 2005) abnormalities have been reported in the LGN and V1 in adults with amblyopia. From V1, we focused on the dorsal white matter projection to area hMT+. This area has a well-established role in the integration of motion information, and is sensitive to binocular disparity (Born & Bradley, 2005; Felleman & Van Essen, 1991; Lewis & Van Essen, 2000; Zeki et al., 1991), functions that are affected by amblyopia (Li et al., 2011; McKee, Levi, & Movshon, 2003; Simmers et al., 2003). Furthermore, functional abnormalities of MT/hMT+ have been reported in both human and non-human primates with amblyopia (Bonhomme et al., 2006; Ho & Giaschi, 2009; El-Shamayleh et al., 2010; Secen et al., 2011; Thompson et al., 2012).

The cortical pathway from V1 to hMT+ is central to conscious perception of visual motion (Cowey, 2010; Rodman, Gross, & Albright, 1989; Schoenfeld, Heinze, & Woldorff, 2002). However, temporary (or even permanent) disruption of V1 activity does not abolish the direction-specific responses to motion in area hMT+ (Cowey, 2010; Cowey & Stoerig, 1991; Zeki & Ffytche, 1998) or MT-MST in macaques (Rodman, Gross, & Albright, 1989, 1990). The fact that visual motion information can still be processed when V1 is lesioned indicates that area hMT+ must receive some input that does not relay through the primary visual cortex.

Indeed, subsequent human and non-human investigations have identified two additional direct thalamic projections to hMT+, which bypass V1 entirely. First, a "subcortical" pathway projects from predominantly koniocellular layers in LGN directly to hMT+ (Sincich et al., 2004). To date, the functional role of this pathway and its role in development and behavior in health and disease has not been determined. A second subcortical pathway connects area hMT+ and the inferior pulvinar nucleus (PLN). Activity in this subcortical visual pathway has been associated with the control of eye movements (Chalupa, Coyle, & Lindsley, 1976; Robinson & McClurkin, 1989), and motion perception (Berman & Wurtz, 2010; Berman & Wurtz, 2011; Casanova et al., 2001; Shipp, 2001). Work in humans suggests that this pathway mediates residual motion perception in blindsight (Cowey, 2010; Intriligator, Xie, & Barton, 2002; Lanyon et al., 2009; Leh et al., 2010; Poppel, Held, & Frost, 1973; Rodman, Gross, & Albright, 1989, 1990; Stoerig & Cowey, 1997), and may underlie Riddoch's phenomenon when conscious motion perception is spared (e.g., Zeki & Ffytche, 1998).

In addition to the thalamo-cortical pathways described above, we also investigated the interhemispheric pathways connecting the left and right hMT+ and V1. These pathways pass through the posterior aspect of the corpus callosum and have been linked to the processing of horizontal motion and anchoring percepts of bistable motion stimuli (Genç et al., 2011).

In the first part of our study, we used DWI and probabilistic tractography to identify the location and diffusion properties of these six early visual pathways in 10 normally sighted participants. By modifying standard techniques for analyzing DWI data, we were able to successfully identify previously difficult to isolate white matter tracts, including the optic radiations and the two subcortical projections to hMT+ that bypass V1 described above. The methodological improvements our protocol offers over traditional DWI tractography methods are considered in the discussion.

We then identified the same six pathways in 10 participants with strabismic, anisometropic or mixed amblyopia. We found significant increases in mean diffusivity within thalamic projections in patients with amblyopia relative to controls. In contrast, no differences were found in cortico-cortical pathways. These results suggest that amblyopia may affect the structural properties of early visual pathways originating in the thalamus.

2. Methods

2.1. Participants

2.1.1. Controls

Ten normally sighted individuals (6 males), aged between 26 and 66 years (mean = 37.3, SD = 13.8), participated as age-matched controls in the study. One participant (male, aged 66 years), whose data contained consistent outliers likely due to excessive head motion, was excluded from the analyses. The next oldest control participant was 65 years old. These participants had normal or corrected-to-normal vision and reported no history of visual disorders.

2.1.2. Participants with amblyopia

Ten individuals (6 males) with amblyopia, aged between 19 and 67 years (mean = 40.6, SD = 14.7), participated in the study. Three had strabismic amblyopia, five anisometropic amblyopia and two mixed amblyopia (both strabismus and anisometropia). Anisometropia was defined as a $\geqslant$1D spherical equivalent difference between the two eyes. Visual acuity was measured using an ETDRS chart viewed from 6 m and stereopsis was measured using the Randot Stereo test (see Table 1 for details). Informed consent was obtained in accordance to the requirements of the IRB review board committee of the University of Auckland. All work was carried out in accordance with the Code of Ethics of the World Medical Association (Declaration of Helsinki).

3. Magnetic resonance imaging

Scans were conducted with a Philips Achieva, 3-T magnetic resonance scanner at Trinity MRI, Auckland, New Zealand equipped with a Phillips 8 Channel head coil. The scanning session included a T1-weighted anatomical scan (2.7 ms TE; 5.8 ms TR; 8° flip angle, 1 mm^3 voxel size) followed by a diffusion-weighted scan (single-shot spin echo EPI, parallel imaging (55 slices)) with 32 measured diffusion directions. Diffusion scans were measured with transverse orientation; AP fold-over direction; TE: 72 ms; TR: 7.139 s; flip angle: 90°; isotropic 2.5 × 2.5 × 2.5 mm^3 resolution; FOV: LR 240 mm × AP 240 mm × FH 137.5 mm; acquisition matrix MxP: 96 × 94; reconstruction matrix 96 × 96; *B* value = 1000; total scan time: 4:02.9 min. We used partial k-space acquisition (SENSE = 2).

4. Data processing

Fig. 1 shows the steps involved in the preprocessing and analysis of the diffusion data.

4.1. Pre-processing & tensor fitting

First, the mean $b = 0$ was computed for the diffusion weighted images, followed by an eddy current correction (with resampling). The corrected DWI data was then aligned to the T1 image. In order to characterize the local properties of the white matter, tensors were fit using the "least-squares" tensor estimation (bootstrapped 500 times; Basser, Mattiello, & LeBihan, 1994). Diffusion imaging pre-processing was performed using vistasoft (Stanford University, Stanford, CA, github.com/vistalab/vistasoft/mrDiffusion). See Fig. 1 panel 1a for an axial view of a representative participant's diffusion weighted imaging data. Tractography visualizations in Fig. 2, panels 4 & 5 were generated with the Matlab Brain Anatomy (MBA)

Table 1
Clinical details of the 10 amblyopic participants. The table reports age (years) and sex for each amblyopic participant, as well as type of amblyopia (anisometropic, strabismic, or mixed), acuity, stereopsis, and refractive error. L = left, R = right.

ID	Age	Sex	Eye	Type of amblyopia	Acuity	Stereo	Correction
A1	29	M	R L	Anisometropia Fellow	20/63 20/20	Nil	4.25 −1.25
A2	32	M	R L	Strabismus Fellow	20/40 20/20	Nil	−0.25 − 0.5 × 90 −0.25 − 0.25 × 90
A3	53	F	R L	Fellow Strabismus	20/20 20/50	Nil	+3.25 − 0.5 × 60 +4 − 0.25 × 120
A4	47	M	R L	Mixed Fellow	20/32 20/15	Nil	+2.5 − 0.25 × 120 +1 − 0.5 × 22
A5	33	M	R L	Mixed Fellow	20/200 20/17	Nil	9.75 −0.25
A6	19	F	R L	Anisometropia Fellow	20/50 20/20	60 arcsec	+3.75 − 1.17 × 180 +0.5 − 0.25 × 180
A7	67	M	R L	Fellow Anisometropia	20/20 20/40	Nil	0.25 +1.5 − 2.25 × 55
A8	51	F	R L	Fellow Anisometropia	20/20 20/50	Nil	+1.25 − 0.25 × 175 +4.75 − 0.5 × 180
A9	47	F	R L	Anisometropia Fellow	20/120 20/20	800 arcsec	−2.25 6
A10	32	M	R L	Strabismus Fellow	20/64 20/20	Nil	0.5 0.25

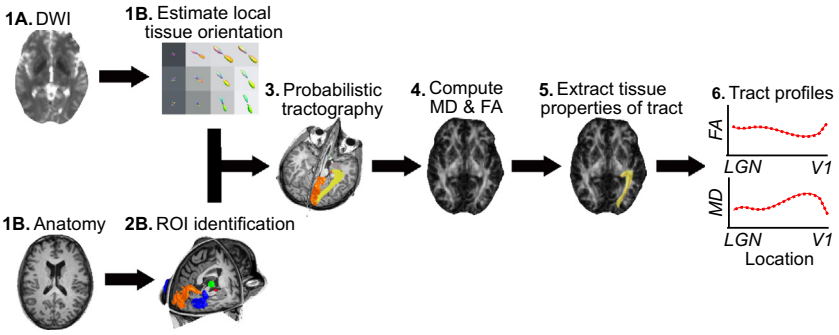

Fig. 1. Steps involved in extracting tissue properties of visual white matter pathways in a representative participant. (1a) Diffusion weighted images (DWI) and (1b) T1-weighted anatomical scans were collected. (2a) Local fiber orientation was estimated using constrained spherical deconvolution. (2b) Regions of interest were identified manually (PLN & LGN; green and red volumes, respectively) and with FreeSurfer auto-segmentation software (V1 & hMT+; orange and blue volumes, respectively). (3) The optic radiation as identified using probabilistic tractography in a representative participant. The orange and red volumes show the end-point ROIs used to constrain the tracking: right V1 (orange) & right LGN (red), respectively. (4) MD and FA were sampled in the voxels composing the estimated pathway (optic radiation shown in yellow). (5) Samples were taken at 100 evenly spaced nodes along the length of the pathway (schematized by red dots). (6) Simulated tract profiles for the right optic radiation in a single participant showing mean diffusivity (MD) and fractional anisotropy (FA) measurements at different nodes along the normalized length of the pathway. MD measures the average distance water diffused in a given voxel. FA is the normalized inverse of MD.

software package (Pestilli et al., 2014; <github.com/francopestilli/mba>).

4.2. ROI identification

The optic chiasm of each participant was identified using gross anatomical landmarks in the T1 image with a fractional anisotropy map overlain. A 2 mm radius sphere was placed in this region to define the chiasmic ROI. Fiber projections from this ROI were estimated using a streamlines tracing technique (STT) (1 mm step size, 30° angle threshold, 0.2 FA threshold, linear interpolation, 15 mm length threshold). The estimated tracts projecting from the chiasm and terminating in the lateral-posterior thalamus provide a reliable marker of LGN location (Basser et al., 2000). A 4 mm radius sphere was placed where the fiber estimates terminated in the lateral thalamus and acted as the LGN ROI. The PLN ROI was a 4 mm sphere placed in the posterior–dorsal aspect of the thalamus identified using gross anatomical landmarks. V1 and hMT+ were identified using the automatic cortical segmentation toolbox in the FreeSurfer software package (Fischl et al., 2002, 2004; Hinds et al., 2007). See Fig. 1 panel 2b for ROIs from a representative participant.

4.3. Fiber tracking

Probabilistic fiber tracking was performed with the MRtrix software package (Brain Research Institute, Melbourne, Australia, <http://www.brain.org.au/software>). Constrained spherical deconvolution (CSD) was used to estimate local fiber orientation. CSD estimates were generated with a maximum spherical harmonic order L_{max} = 6. CSD-based probabilistic tractography can produce connectome models that are well matched to the measured diffusion signal (Pestilli et al., 2014). See Fig. 1 panel 2a for CSD models generated from a small subset of DWI voxels in a representative participant. Pathway estimates were generated by seeding all voxels in a specified ROI and probabilistically tracking until the tracking parameters

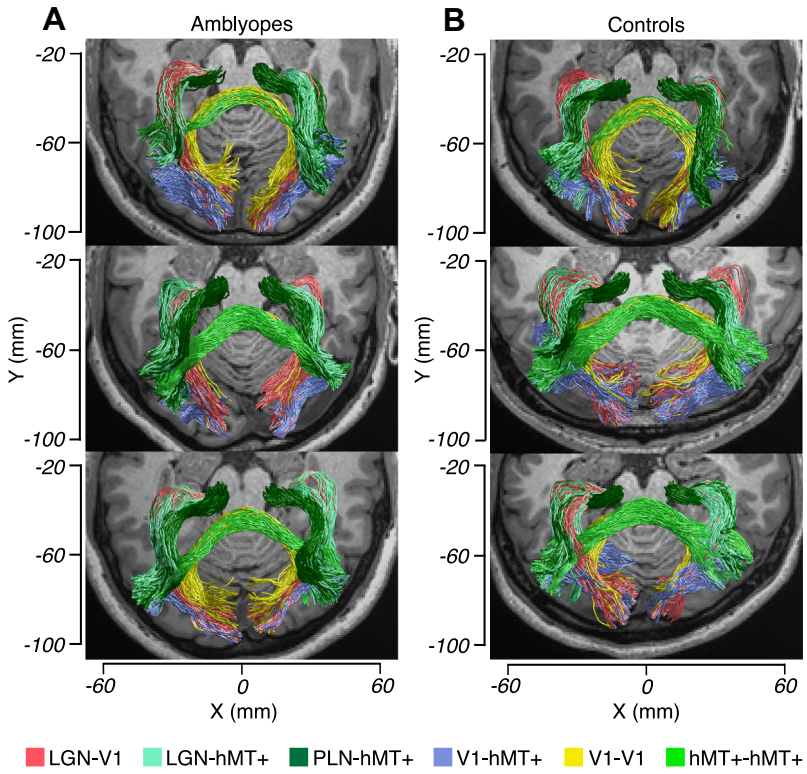

Fig. 2. Visual white matter pathways estimated by probabilistic tractography in representative participants with amblyopia (A) and controls (B). LGN = lateral geniculate nucleus; PLN = pulvinar nucleus. Each pathway is color-coded.

could no longer be satisfied. Only fibers terminating in the end-pair ROI were used for pathway estimation. Hemisphere-specific white matter masks of the posterior half of each brain were used to constrain pathway estimates to intrahemisphere white matter in the lobes of interest. A white matter mask of the posterior half of both hemispheres was used to anatomically constrain the fiber tracking when estimating interhemisphere fibers connecting left and right V1 and hMT+. A more detailed description of this probabilistic tractography protocol is provided in the "Fiber-tracking" section of Calamante et al. (2011).

4.4. Fiber cleaning

Once the initial pathway estimates were created, we removed any fibers that were unlikely to belong to the pathway of interest using the Automated Fiber Quantification software package (Yeatman et al., 2012). In short, the software computes the average distance between the individual fibers and removes any fibers (1) whose average distance from its neighbors is greater than 4 standard deviations or (2) shorter than 20 nodes. These "cleaned" fibers were then manually inspected for abnormalities. In one control participant, 10 fibers, which passed through CSF, were manually removed. The resulting fibers were used as the final pathway estimates (see Fig. 1 panel 3 for an optic radiation estimate from a representative participant).

4.5. Diffusion measures

We characterized the white matter by computing two measures based on the tensor fit to the diffusion signal from individual voxels: mean diffusion (MD) and fractional anisotropy (FA). Mean diffusivity reflects how freely water diffuses in a given part of the brain and is a measure of diffusion magnitude. Smaller MD values indicate more restricted diffusion of water, indicating greater tissue density and/or increased myelination in the associated tissue. Fractional anisotropy is a measure of diffusion directionality (the normalized inverse of MD), indicating how freely water diffuses in one direction, relative to the 2 other perpendicular directions.

4.6. Tract-based analysis of diffusion measures

Mean MD and FA measures for each pathway were obtained for each participant. Since pathway length varied between participants, we normalized the number of samples obtained for each pathway by sampling 100 evenly spaced cross-sectional nodes along the length of the fiber estimates (Fig. 1, panels 4 & 5). This approach is part of vistasoft (github.com/vistalab/vistasoft) and has been described in detail in the context of the AFQ package (Yeatman et al., 2012). Only the middle 60% of samples taken along the normalized length of the fibers were used for analysis to ensure that the dataset included only unambiguous white matter and not voxels at the gray/white matter interface. This was a particular concern, as gray matter abnormalities may exist in patients with amblyopia (Barnes et al., 2010; Lv et al., 2008).

The resulting 60 samples for both the left and right tracts of each pathway were combined, generating a single set of 120 samples for each pathway of interest for each participant. We then averaged across these 120 samples for each participant to provide a single-value estimate of the average properties of a given pathway for each participant. A mixed-factor ANOVA was used to test for main effects of group (participants with amblyopia versus controls), pathway, and interaction between the two factors. In addition, post hoc independent-sample *t*-tests were used to compare the mean MD and FA measures for each pathway between participants with amblyopia and controls. See Fig. 3 for a plot of the difference in MD and FA between amblyopes and controls for each pathway considered.

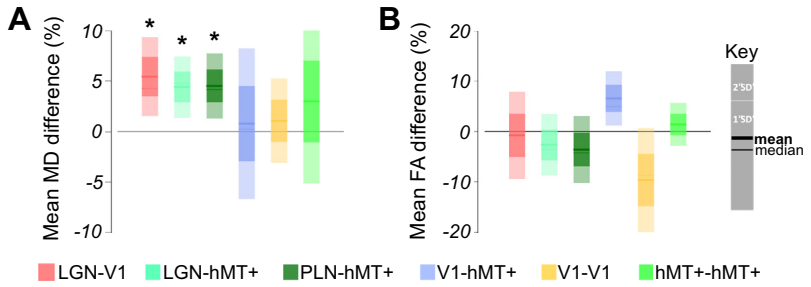

Fig. 3. Percent differences in mean (A) MD and (B) FA between amblyopes and controls for the six white matter pathways of interest. Thick horizontal lines show group mean differences, thin horizontal lines show group median differences. Darker and lighter regions show one and two standard deviations from the mean differences, respectively. Data are averaged across hemisphere. Positive differences indicate amblyopes show greater MD/FA than controls. $^{*}p < 0.05$.

5. Results

5.1. Anatomy of the early visual pathways

We successfully identified the six pathways of interest in all participants using constrained spherical deconvolution paired with probabilistic tractography. Fig. 2 shows pathway anatomy estimates for six representative participants (three participants with amblyopia and three controls).

5.2. Comparisons between controls and participants with amblyopia

For the MD data, a mixed-factor ANOVA revealed a significant main effect of both group (amblyopes vs. controls) ($F_{1,5} = 5.43$, $p = 0.032$), and pathway ($F_{1,5} = 28.89$, $p < 0.0001$) but no interaction between the two factors ($F_{1,5} = 0.60$, $p = 0.70$). No main effects or interactions were observed for the FA data ($F_{1,5} < 3$, $p > 0.05$ for all comparisons).

Post hoc t-tests revealed significant differences in MD between amblyopes and controls within all three thalamocortical tracts (LGN–V1: $t_{17} = 3.80$, $p < 0.002$; LGN–hMT+: $t_{17} = 3.57$, $p < 0.005$; and PLN–hMT+: $t_{17} = 3.44$, $p < 0.005$). As shown in Fig. 3, amblyopes exhibited greater MD in the thalamocortical tracts than controls. Representative anatomy estimates for these three thalamocortical pathways are shown in Fig. 4 along with group-averaged tract profiles showing the differences in mean MD across the length of these pathways (middle and bottom).

No significant differences were found for MD values within the cortico-cortical tracts (V1–hMT+, V1–V1, and hMT–hMT+ ($t_{17} < 1.5$, $p > 0.05$, for all pathways; Fig. 5). In addition, no differences were found for FA values for any tracts ($p > 0.05$; Fig. 3B).

Finally, we found no significant correlations between white matter properties (in individual pathways or averaging across all pathways) and visual acuity, age, gender or type of amblyopia (all $p > 0.05$). While age-related diffusion differences have been observed, our experimental groups are closely age-matched and mean age did not differ significantly between the two groups, suggesting our results are likely not confounded by age related differences. Finally, we found no significant differences in mean MD or mean FA in pathways contra- versus ipsi-lateral to the amblyopic eye (all $p > 0.05$).

6. Discussion

6.1. Methodological advances in tracking the early visual pathways

First, we assessed whether novel DWI techniques could identify six pre-specified white matter tracts within the human visual system. By combining constrained spherical deconvolution (CSD) and probabilistic tractography, all six of the pathways could be identified. Probabilistic tractography methods such as the one used here have been recently shown to produce superior mapping of white-matter pathways (Pestilli et al., 2014). Previous reports using tensor-based deterministic tractography methods (i.e., streamline tracing techniques, STT) failed to identify some of the pathways under investigation, including the pathway between the LGN and hMT+ (Lanyon et al., 2009). In an initial investigation, we replicated this limitation. Specifically, we were unable to identify several of the callosal and thalamo-cortical pathways in the majority of participants. CSD-based fiber tracking offers major advances over traditional tensor-based tracking (Pestilli et al., 2014; Tournier et al., 2008). Primarily, because CSD allows for the modeling of multiple fiber orientations in a single voxel, CSD-based probabilistic tractography is more robust in regions of the white matter that contain both parallel and tangential fiber crossings (Tournier et al., 2008). It should be noted that the addition of each new local fiber orientation to a CSD estimate comes with a cost function. Thus, greater numbers of DWI scan directions will not necessarily result in CSD estimates that provide greater numbers of local fiber orientations.

Although significant differences were found between amblyopes and controls for MD, we did not find such differences for FA. FA values were much more variable both within and between participants. While we did observe trends in the data such that FA and MD showed opposite patterns (FA is the normalized inverse of MD), the absence of any significant effects of FA in our analysis is likely due to the larger variability inherent to fractional measures.

6.2. Abnormal visual white matter properties in amblyopia

Secondly, we tested whether amblyopia is associated with abnormal white matter structure. We found that participants with amblyopia exhibited larger MD values (greater diffusivity) in the LGN–V1, the LGN–hMT+ and the PLN–hMT+ pathways. These effects were not present in cortico-cortical tracts. Increased MD values may be associated with decreased axonal density, decreased myelination, and/or less orderly organization of white matter axons (see Alexander et al., 2012 for an in-depth review of the anatomical properties associated with DWI measures). Therefore our results suggest that white matter tracts at an early, thalamic stage of the visual pathway are affected by amblyopia. This idea is consistent with previous reports of abnormal LGN structure (Barnes et al., 2010) and function (Hess et al., 2009, 2010; Miki et al., 2003) in humans with amblyopia. In addition, reduced feed forward and feedback connectivity between the LGN and V1 has been demonstrated for adults with amblyopia (Li et al., 2010) as well as abnormal patterns of functional activity within the PLN (Thompson et al., 2012). Our results suggest that these functional and structural changes affecting thalamic areas in patients with amblyopia also involve impaired white matter development.

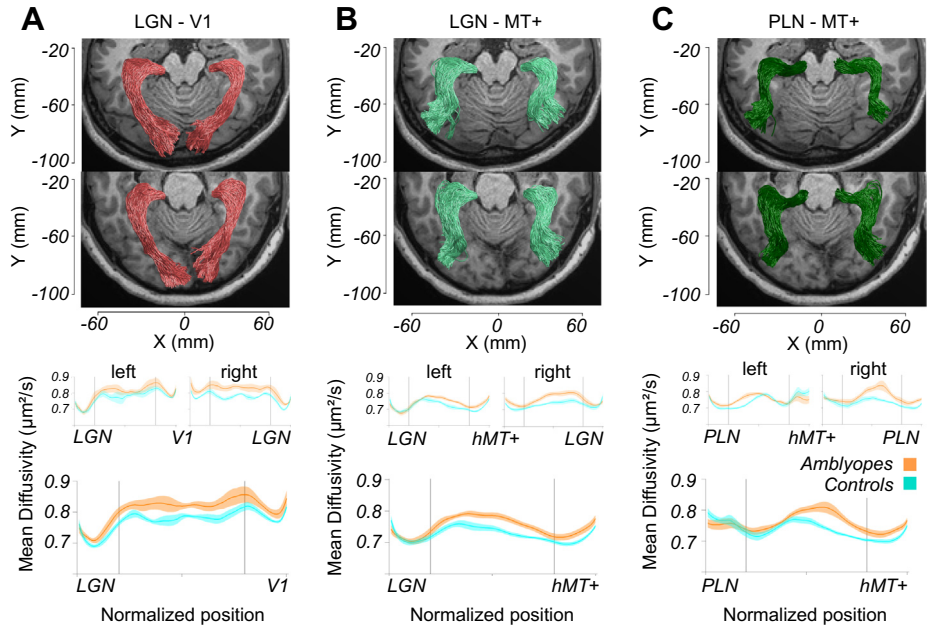

Fig. 4. Representative anatomy and tract profiles of the three thalamo-cortical pathways of interest. (A), (B), & (C) Top: visualized pathway anatomy estimates in one representative control (top) and one representative amblyopic (bottom) participant of the three thalamo-cortical pathways. Middle: hemisphere-specific group tract profiles for the left and right pathways. Bottom: hemisphere-averaged group tract profiles showing the mean MD across the normalized length of the pathways. Vertical lines define the middle 60% of the normalized pathway positions used for statistical comparisons. All three pathways show significantly increased mean diffusivity in amblyopes compared to controls.

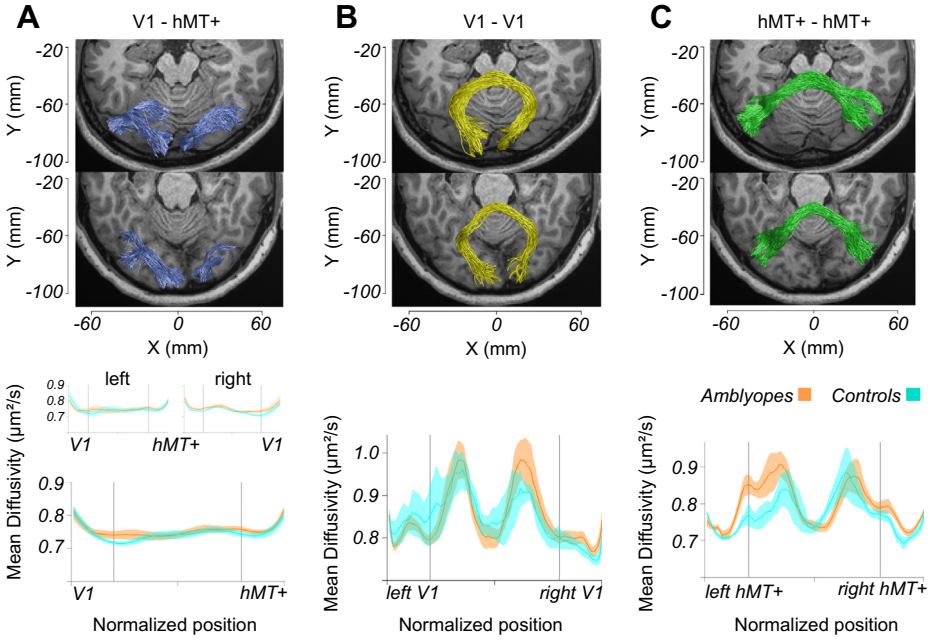

Fig. 5. Representative anatomy and tract profiles of the three cortico-cortical pathways of interest. (A), (B), & (C) Top: visualized pathway anatomy estimates in one representative control (top) and one representative amblyopic (bottom) participant for the three cortico-cortical pathways. (A) Middle: hemisphere-specific group tract profiles for the left and right pathways. (A) Bottom: hemisphere-averaged group tract profiles showing the mean MD across the normalized length of the pathways. (B) & (C) Bottom: group tract profiles showing the mean MD across the normalized length of the two callosal cortico-cortical pathways. Vertical lines define the middle 60% of the normalized pathway positions used for statistical comparisons. None of these pathways showed significant differences in diffusion measures between amblyopes and controls.

Unfortunately, the number of amblyopic participants in our study prevents us from separately characterizing the effects of strabismic versus anisometropic amblyopia on white matter structure. Therefore, the degree to which the individual symptoms of amblyopia may affect the white matter is open to future investigation.

6.3. Anatomical limitations and implications

To our knowledge, this is the first study to identify white matter pathways connecting both the LGN and PLN of the thalamus to extrastriate area hMT+ in humans reliably *in vivo*. While tractography is vulnerable to false-positive pathway identification (Thomas

et al., 2014), these pathway estimates do provide evidence for direct thalamic connections with area hMT+ in humans akin to those found in non-human primates. Further tractography quantification analyses as well as *ex vivo* studies are needed to support these findings.

An active research question in tractography and diffusion imaging is the degree to which white-matter fibers (and the tracts they pertain to) cross in the brain. Recent reports have shown that a majority of white-matter may very well comprise multiple coexisting tracts whose properties are difficult to disentangle (Jeurissen et al., 2012; Pestilli et al., 2014; Vos et al., 2012; Wedeen et al., 2012). This has important implications for our work, especially because several of the pathways we discuss overlap anatomically, as can be seen in Fig. 2. In addition to the pathways we have studied, other pathways coexist within the same portion of the white matter (notable examples are the inferior front occipital fasciculus and the inferior lateral fasciculus, Yeatman et al., 2012).

The thalamic ROIs in this study were identified based on relatively easily discriminable anatomical landmarks and deterministic DWI techniques. In the absence of functional localizers, the cortical ROIs were identified using the automatic cortical segmentation toolbox in the FreeSurfer software package. Visual inspection of the cortical ROIs revealed them to correspond closely to their known location and morphology, although we cannot exclude the possibility that the method of ROI identification provides somewhat different results for participants with amblyopia versus controls.

More generally, the multi-millimeter voxel resolution of our diffusion scans coupled with the partially overlapping nature of the three thalamo-cortical pathways, means that we cannot exclude concerns regarding the independence of the findings in these three pathways. While our findings highlight the need to further develop techniques to parcel out the white matter properties of specific pathways, we can conclude that there is significantly increased diffusivity in visual white matter regions occupied by these thalamo-cortical visual pathways, which is likely the consequence of the effects of amblyopia on neural development.

Acknowledgments

This work was supported by Grants from the Auckland Medical Research Foundation, the University of Auckland Faculty Research Development Fund and the Health Research Council of New Zealand to BT, the Worldwide Universities Network (WUN) to BT and BR, and the Wisconsin Alumni Research Foundation (WARF) to BR. FP was funded by grants to Brian Wandell (Stanford University) NEI EY015000 and NSF BCS-1228397.

References

Alexander, A., Hurley, S., Samsonov, A., Adluru, N., Hosseinbor, A., Pouria, M., et al. (2012). Characterization of cerebral white matter properties using quantitative magnetic resonance imaging stains. *Brain Connectivity, 1*(6), 423–446.

Asper, L., Crewther, D., & Sheila, C. (2000). Strabismic amblyopia. *Clinical and Experimental Optometry, 83*(2), 49–58.

Barnes, G., Li, X., Thompson, B., Singh, K., Dumoulin, S., & Hess, R. (2010). Decreased gray matter concentration in lateral geniculate nuclei in human amblyopes. *Investigative Ophthalmology & Visual Science, 51*(3), 1432–1438.

Basser, P. J., Mattiello, J., & LeBihan, D. (1994). MR diffusion tensor spectroscopy and imaging. *Biophysical Journal, 66*, 259–267.

Basser, P. J., Pajevic, S., Pierpaoli, C., Duda, J., & Aldroubi, A. (2000). In vivo fiber tractography using DT-MRI data. *Magnetic Resonance in Medicine, 44*, 625–632.

Berman, R. A., & Wurtz, R. H. (2010). Functional identification of a pulvinar path from superior colliculus to cortical area MT. *Journal of Neuroscience, 30*(18), 6342–6354.

Berman, R. A., & Wurtz, R. H. (2011). Signals conveyed in the pulvinar pathway from superior colliculus to cortical area MT. *Journal of Neuroscience, 31*(2), 373–384.

Bonhomme, G., Liu, G., Miki, A., Francis, E., Dobre, M., Modestino, E., et al. (2006). Decreased cortical activation in response to a motion stimulus in anisometropic amblyopic eyes using functional magnetic resonance imaging. *Journal of American Association for Pediatric Ophthalmology and Strabismus, 10*(6), 540–546.

Born, R., & Bradley, D. (2005). Structure and function of visual area MT. *Annual Review of Neuroscience, 28*, 157–189.

Calamante, F., Tournier, J., Heidermann, R., Anwander, A., Jackson, G., & Connelly, A. (2011). Track density imaging (TDI): Validation of super resolution property. *NeuroImage, 3*(1), 1259–1266.

Casanova, C., Merabet, L., Desautels, A., & Minville, K. (2001). Higher-order motion processing in the pulvinar. *Progress in Brain Research, 134*, 71–82.

Chalupa, L., Coyle, R., & Lindsley, D. (1976). Effect of pulvinar lesions on visual pattern discrimination in monkeys. *Journal of Neurophysiology, 39*, 354–369.

Chan, S., Tang, K., Lam, K., Chan, L., Mendola, J., & Kwong, K. (2004). Neuroanatomy of adult strabismus: A voxel-based morphometric analysis of magnetic resonance structural scans. *Neuroimage, 22*(2), 986–994.

Cowey, A. (2010). Visual system: How does blindsight arise? *Current Biology, 20*(17), R702–R704.

Cowey, A., & Stoerig, P. (1991). The neurobiology of blindsight. *Trends in Neurosciences, 14*, 140–145.

El-Shamayleh, Y., Kiorpes, L., Kohn, A., & Movshon, J. A. (2010). Visual motion processing by neurons in area MT of macaque monkeys with experimental amblyopia. *Journal of Neuroscience, 30*(36), 12198–12209.

Felleman, D., & Van Essen, D. (1991). Distributed hierarchical processing in the primate cerebral cortex. *Cerebral Cortex, 1*, 1–47.

Fischl, B., Salat, D., Busa, E., Albert, M., Dietrich, M., Haselgrove, C., et al. (2002). Whole brain segmentation: Automated labeling of neuroanatomical structures in the human brain. *Neuron, 3*(31), 341–355.

Fischl, B., van der Kouwe, A., Destrieux, C., Halgren, E., Segonne, F., Salat, D., et al. (2004). Automatically parcellating the human cerebral cortex. *Cerebral Cortex, 14*(1), 11–22.

Genç, E., Bergmann, J., Singer, W., & Kohler, A. (2011). Interhemispheric connections shape subjective experience of bistable motion. *Current Biology, 21*(17), 1494–1499.

Gümüstas, S., Altintas, O., Anik, Y., Kaya, A., Altintas, L., Inan, N., et al. (2013). Anterior visual pathways in amblyopia: Quantitative assessment with diffusion tensor imaging. *Journal of Pediatric Ophthalmology and Strabismus, 50*(6), 369–374.

Hamm, L., Black, J., Dai, S., & Thompson, B. (2014). Global processing in amblyopia: A review. *Frontiers in Psychology, 5*, 1–21.

Hess, R. F., & Howell, E. R. (1977). The threshold contrast sensitivity function in strabismic amblyopia: Evidence for a two type classification. *Vision Research, 17*(9), 1049–1055.

Hess, R., Thompson, B., Gole, G., & Mullen, K. (2009). Deficient responses from the lateral geniculate nucleus in humans with amblyopia. *European Journal of Neuroscience, 29*(5), 1064–1070.

Hess, R., Thompson, B., Gole, G., & Mullen, K. (2010). The amblyopic deficit and its relationship to geniculo-cortical processing streams. *Journal of Neurophysiology, 104*(1), 475–483.

Hinds, O., Rajendran, N., Polimeni, J., Augustinack, J., Wiggins, G., Wald, L., et al. (2007). Accurate prediction of V1 location from cortical folds in a surface coordinate system. *NeuroImage, 39*(4), 1585–1599.

Ho, C. S., & Giaschi, D. E. (2009). Low- and high-level motion perception deficits in anisometropic and strabismic amblyopia: Evidence from fMRI. *Vision Research, 49*, 2891–2901.

Holmes, J., & Clarke, M. (2006). Amblyopia. *The Lancet, 367*(9519), 1343–1351.

Hubel, D. H., & Wiesel, T. N. (1970). The period of susceptibility to the physiological effects of unilateral eye closure in kittens. *Journal of Physiology, 206*, 419–436.

Intriligator, J., Xie, R., & Barton, J. (2002). Blindsight modulation of motion perception. *Journal of Cognitive Neuroscience, 14*, 1174–1183.

Jeurissen, B., Leemans, A., Tournier, J., Jones, D., & Sijbers, J. (2012). Investigating the prevalence of complex fiber configurations in white matter tissue with diffusion magnetic resonance imaging. *Human Brain Mapping, 34*(11), 2747–2766.

Lanyon, L., Giaschi, D., Au Young, S., Fitzpatrick, K., Diao, L., Bjornson, B., et al. (2009). Combined functional MRI and diffusion tensor imaging analysis of visual motion pathways. *Journal of Neuro-Ophthalmology, 29*, 96–103.

Leh, S., Ptito, A., Schonwiesner, M., Chakravarty, M., & Mullen, K. (2010). Blindsight mediated by an S-cone-independent collicular Pathway: An fMRI Study in hemispherectomized subjects. *Journal of Cognitive Neuroscience, 22*, 670–682.

Levi, D. M., & Harwerth, R. S. (1978). Contrast evoked potentials in strabismic and anisometropic amblyopia. *Investigative Ophthalmology & Visual Science, 17*(6), 571–575.

Levi, D. M., & Klein, S. (1982). Hyperacuity and amblyopia. *Nature, 298*(5871), 268–270.

Lewis, J., & Van Essen, D. (2000). Corticocortical connections of visual, sensorimotor, and multimodal processing areas in the parietal lobe of the macaque monkey. *The Journal of Comparative Neurology, 428*(1), 112–137.

Li, X., Mullen, K., Thompson, B., & Hess, R. (2010). Effective connectivity anomalies in human amblyopia. *NeuroImage, 54*(1), 505–516.

Li, J., Thompson, B., Lam, C. S., Deng, D., Chan, L. Y., Maehara, G., et al. (2011). The role of suppression in amblyopia. *Investigative Ophthalmology & Visual Science, 52*(7), 4169–4176.

Lv, B., He, H., Li, X., Zhang, Z., Huang, W., Li, M., et al. (2008). Structural and functional deficits in human amblyopia. *Neuroscience Letters, 437*(1), 5–9.

McKee, S., Levi, D., & Movshon, J. (2003). The pattern of visual deficits in amblyopia. *Journal of Vision, 3*(5), 1–26.

Mendola, J., Conner, I., Roy, A., Chan, S., Schwartz, T., Odom, J., et al. (2005). Voxel-based analysis of MRI detects abnormal visual cortex in children and adults with amblyopia. *Human Brain Mapping, 25*(2), 222–236.

Movson, J., Eggers, H., Gizzi, M., Hendrickson, A., Kiorpes, L., & Boothe, R. (1987). Effects of unilateral blur on the macaque's visual system. III. Physiological observations. *The Journal of Neuroscience, 7*(5), 1340–1351.

Miki, A., Liu, G., Goldsmith, Z., Liu, C., & Haselgrove, J. (2003). Decreased activation of the lateral geniculate nucleus in a patient with anisometropic amblyopia demonstrated by functional magnetic resonance imaging. *Ophthalmologica, 217*(5), 365–369.

Ming-xia, G., Yun-ting, Z., Quan, Z., & Wei, L. (2007). Study on the optic radiation disruption in children ametropic, anisometropic, and strabismic amblyopia by DTI and DTT. *International Conference on Complex Medical Engineering*, 1371–1374.

Mizoguchi, S., Suzuki, Y., Kiyosawa, M., Mochizuki, M., & Ishii, K. (2005). Differential activation of cerebral blood flow by stimulating amblyopic and fellow eye. *Graefe's Archive for Clinical and Experimental Ophthalmology, 243*, 576–584.

Pestilli, F., Yeatman, J., Rokem, A., Kay, K., & Wandell, B. (2014). Evaluation and statistical inference for human connectomes. *Nature Methods*.

Pineles, S., & Demer, J. (2009). Bilateral abnormalities of optic nerve size and eye shape in unilateral amblyopia. *American Journal of Ophthalmology, 148*(4), 551–557.

Poppel, E., Held, R., & Frost, D. (1973). Residual visual function after brain wounds involving the central visual pathways in man. *Nature, 243*, 295–296.

Robinson, D., & McClurkin, J. (1989). The visual superior colliculus and pulvinar. *Reviews of Oculomotor Research, 3*, 337–360.

Rodman, H., Gross, C., & Albright, T. (1989). Afferent basis of visual response properties in area MT of the macaque. I. Effects of striate cortex removal. *The Journal of Neuroscience, 9*, 2033–2050.

Rodman, H., Gross, C., & Albright, T. (1990). Afferent basis of visual response properties in area MT of the macaque. II. Effects of superior colliculus removal. *Journal of Neuroscience, 10*, 1154–1164.

Schoenfeld, M. A., Heinze, H.-J., & Woldorff, M. G. (2002). Unmasking motion-processing activity in human brain area V5/MT+ mediated by pathways that bypass primary visual cortex. *NeuroImage, 17*(2), 769–779.

Secen, J., Culham, J., Ho, C., & Giaschi, D. (2011). Neural correlates of the multiple-object tracking deficit in amblyopia. *Vision Research, 51*, 2517–2527.

Shipp, S. (2001). Corticopulvinar connections of areas V5, V4, and V3 in the macaque monkey: A dual model of retinal and cortical topographies. *Journal of Comparative Neurology, 439*, 469–490.

Simmers, A. J., Ledgeway, T., Hess, R. F., & McGraw, P. V. (2003). Deficits to global motion processing in human amblyopia. *Vision Research, 43*, 729–738.

Sincich, L., Park, K., Wohlgemuth, M., & Horton, J. (2004). Bypassing V1: A direct geniculate input to area MT. *Nature Neuroscience, 7*(10), 1123–1128.

Song, H., Qi, S., Tang, H., Yu, F., & Liu, L. (2010). MR DTI and DTT study on the development of optic radiation in patients with anisometropia amblyopia. *Journal of Sichuan University. Medical Science Edition, 41*(4), 648–651.

Stoerig, P., & Cowey, A. (1997). Blindsight in man and monkey. *Brain, 120*, 535–559.

Thomas, C., Frank, Q. Y., Irfanoglu, M. O., Modi, P., Saleem, K. S., Leopold, D. A., et al. (2014). Anatomical accuracy of brain connections derived from diffusion MRI tractography is inherently limited. *Proceedings of the National Academy of Sciences, 111*(46), 16574–16579.

Thompson, B., Villeneuve, M. Y., Casanova, C., & Hess, R. F. (2012). Abnormal cortical processing of pattern motion in amblyopia: Evidence from fMRI. *NeuroImage, 60*(2).

Tournier, J., Yeh, C., Calamante, F., Cho, K., Connelly, A., & Lin, C. (2008). Resolving crossing fibres using constrained spherical deconvolution: Validation using diffusion-weighted imaging phantom data. *NeuroImage, 42*, 617–625.

von Noorden, G., Crawford, M., & Levacy, R. (1983). The lateral geniculate nucleus in human anisometropic amblyopia. *Investigative Ophthalmology & Visual Science, 24*(6), 788–790.

Vos, S., Jones, D., Jeurissen, B., Viergever, M., & Leemans, A. (2012). The influence of complex white matter architecture on the mean diffusivity in diffusion tensor MRI of the human brain. *Neuroimage, 59*(3), 2208–2216.

Wedeen, V., Rosene, D., Wang, R., Dai, G., Mortazavi, F., Hagmann, P., et al. (2012). The geometric structure of the brain fiber pathways. *Science, 335*(6076), 1628–1634.

Xie, S., Gong, G., Xiao, J., Ye, J., Liu, H., Gan, X., et al. (2007). Underdevelopment of optic radiation in children with amblyopia: A tractography study. *American Journal of Ophthalmology, 143*(4), 642–646.

Yeatman, J., Dougherty, R., Myall, N., Wandell, B., & Feldman, H. (2012). Tract profiles of white matter properties: Automating fiber-tract quantification. *PLoS ONE, 7*(11), e49790.

Zeki, S., Watson, J., Lueck, C., Friston, K., Kennard, C., & Frackowaik, R. (1991). A direct demonstration of functional specialization in human visual cortex. *The Journal of Neuroscience, 11*(3), 641–649.

Zeki, S., & Ffytche, D. (1998). The Riddoch syndrome: Insights into the neurobiology of conscious vision. *Brain, 121*(1), 25–45.